The Journal of Experimental Biology 215, 1766-1774

doi:10.1242/jeb.067355

RESEARCH ARTICLE

Neuromuscular control of free-flight yaw turns in the hawkmoth *Manduca sexta*

Dwight Springthorpe[1], María José Fernández[2] and Tyson L. Hedrick[2,*]

[1]Department of Integrative Biology, University of California, Berkeley, Berkeley, CA 94720, USA and [2]University of North Carolina at Chapel Hill, Chapel Hill, NC 27599, USA

*Author for correspondence (thedrick@bio.unc.edu)

Accepted 3 February 2012

SUMMARY

The biomechanical properties of an animal's locomotor structures profoundly influence the relationship between neuromuscular inputs and body movements. In particular, passive stability properties are of interest as they may offer a non-neural mechanism for simplifying control of locomotion. Here, we hypothesized that a passive stability property of animal flight, flapping counter-torque (FCT), allows hawkmoths to control planar yaw turns in a damping-dominated framework that makes rotational velocity directly proportional to neuromuscular activity. This contrasts with a more familiar inertia-dominated framework where acceleration is proportional to force and neuromuscular activity. To test our hypothesis, we collected flight muscle activation timing, yaw velocity and acceleration data from freely flying hawkmoths engaged in planar yaw turns. Statistical models built from these data then allowed us to infer the degree to which the moths inhabit either damping- or inertia-dominated control domains. Contrary to our hypothesis, a combined model corresponding to inertia-dominated control of yaw but including substantial damping effects best linked the neuromuscular and kinematic data. This result shows the importance of including passive stability properties in neuromechanical models of flight control and reveals possible trade-offs between manoeuvrability and stability derived from damping.

Supplementary material available online at http://jeb.biologists.org/cgi/content/full/215/10/1766/DC1

Key words: flight, stability, neuromechanical, manoeuvring, insect.

INTRODUCTION

Animals are highly successful at navigating their environments and achieve remarkable manoeuvrability and stability using locomotor mechanisms that, in most cases, differ substantially from those of human-engineered vehicles. These abilities arise, at least in part, from the interaction of the organisms' unique biomechanical properties and their neural control mechanisms (Dickinson et al., 2000; Nishikawa et al., 2007). For instance, investigations into terrestrial arthropod locomotion have shown that the properties of the mechanical (Full et al., 1998; Sponberg and Full, 2008) and sensory systems (Cowan et al., 2006) can simplify control of locomotion (Cowan and Fortune, 2007). In this study, we extend neuromechanical investigation of control of animal movement to flight, showing how aerodynamic damping influences neuromuscular control of turning in freely flying hawkmoths.

A flying animal turns by applying an asymmetric aerodynamic torque, τ. This input is related to the animal's rotational acceleration, $\dot{\omega}$, and moment of inertia, I, by the following equation:

$$\dot{\omega} = \frac{1}{I}\tau \ . \tag{1}$$

This is related to the animal's rotational velocity, $\boldsymbol{\omega}$, at a given time, t, by the following:

$$\boldsymbol{\omega}(t) = \frac{1}{I}\int_0^t \tau(t)\mathrm{d}t \ . \tag{2}$$

In this case, the animal's current velocity depends on all previously applied torques. For instance, a turn from one heading to another requires two distinct impulses: one to initiate the turn and a second in the opposite direction that must be applied midway through the turn if the animal is to avoid overshooting its intended heading (Åström and Murray, 2008). However, a recently proposed passive stability mechanism for flapping flight, flapping counter-torque (FCT), may permit some flying animals to use a different approach to control aerial locomotion by altering the interaction of wing and body dynamics with neuromuscular inputs (Hedrick and Robinson, 2010).

FCT results from differences in wing motion relative to the surrounding fluid due to body rotation (Hedrick et al., 2009). The resulting damping force is inversely proportional to the flapping animal's instantaneous yaw velocity and is related to the animal's kinematics and actively applied rotational torques by the following equation:

$$\dot{\omega} = \frac{1}{I}(\tau - b_\omega \boldsymbol{\omega}) \ . \tag{3}$$

For a constantly applied torque, this has an analytic solution:

$$\boldsymbol{\omega}(t) = \frac{\tau}{b_\omega}\left(1 - e^{-\frac{b_\omega t}{I}}\right) \ . \tag{4}$$

In Eqns 3 and 4, b_ω is a constant coefficient that combines various morphological and kinematic factors which are unique to each species, individual and behaviour [for further information on b_ω, see Hedrick et al. (Hedrick et al., 2009)]. For a constant torque, yaw velocity will asymptotically approach a saturation velocity, ω_s that is equal to τ/b_ω with a half-life of $\ln(2)I\,b_\omega^{-1}$. Half-lives of between 10 and 40 ms, as predicted by current models of FCT in a variety

of flying animals (Hedrick et al., 2009), can produce substantial differences in body dynamics from comparable undamped systems (Fig. 1A) at an assumed control input time scale for flying insects of one or more wingbeats.

If the transient effects of this damping are short compared with the rate at which the animal varies the input torque [i.e. the frequency at which $\tau(t)$ changes], then the resultant angular velocity will be effectively proportional to the input torque, reducing Eqn 4 to:

$$\boldsymbol{\omega}(t) = \frac{\tau(t)}{b_{\omega}} . \quad (5)$$

This shift to a damping-dominated system, which can equally be created by increasing b_{ω}, decreasing I or reducing the input frequency at which $\tau(t)$ varies, may be desirable because it reduces the amount of information and computation required for motion (Fig. 1B,C). Such a system may also facilitate sensor–motor integration as the visual systems in many animals have well-known linear responses to velocity stimuli (e.g. Fry et al., 2009; Orban et al., 1985). This postulated direct relationship from muscle activation asymmetry to angular velocity is also characteristic of low-speed roll manoeuvres in cockatiels (Hedrick and Biewener, 2007a), another case where damping is likely to play a large role in flight control.

The importance of FCT to the control of yaw orientation is supported by recent work. Fruit flies, when subjected to unexpected rotational perturbations, use passive damping to halt rotation for both the perturbation and their active recovery. Counter-rotational damping thus allows the flies to adopt a recovery strategy where the response consists of only a rotational impulse equal and opposite to that of the perturbation (Ristroph et al., 2010).

However, the presence of damping also introduces a penalty to locomotor energy efficiency in a manner analogous to normal fluid drag. To perform a given manoeuvre, the flying animal must expend energy not only to overcome its inertia but also to counteract damping. FCT damping and its associated effects on the control of movement may thus represent a compromise between stability and potentially simplified control on the one hand and locomotor energy efficiency and manoeuvrability on the other.

To assess the degree to which the passive damping properties affect flight control and provide insight into the possible manoeuvrability/stability compromises with which flying animals contend, we correlated muscle activation patterns and task-level kinematics of freely flying hawkmoths engaged in planar yaw turns. Although we are unable to directly assess the neural control of these voluntary manoeuvres at their origin in the central nervous system, we are able to infer general characteristics of the control framework by measuring neuromuscular activation patterns and external kinematics. Hawkmoths perform voluntary yaw turns by producing asymmetric aerodynamic forces that, in turn, are the product of asymmetric activation of the insect's flight muscles. As bilateral activation timing differences in these muscles are correlated with mechanical power output (Josephson, 1985), asymmetric flapping kinematics (e.g. Balint and Dickinson, 2004) and yaw torque production (Sponberg and Daniel, 2010), we can assess the magnitude of the hawkmoth's turning input by acquiring neuromuscular activation data from bilateral pairs of flight muscles.

The substantial passive damping observed in hawkmoths (Hedrick and Robinson, 2010) led us to hypothesize that they exhibit a damping-dominated yaw control architecture. In this case, a model that correlates observed yaw velocity and muscle activation timing differences will best fit the observed yaw turn kinematics during individual wingbeats. Alternatively, a model correlating yaw acceleration (or wingbeat to wingbeat changes in velocity) with muscle activation will better fit the observed kinematics for a hawkmoth with inertia-dominated plant dynamics.

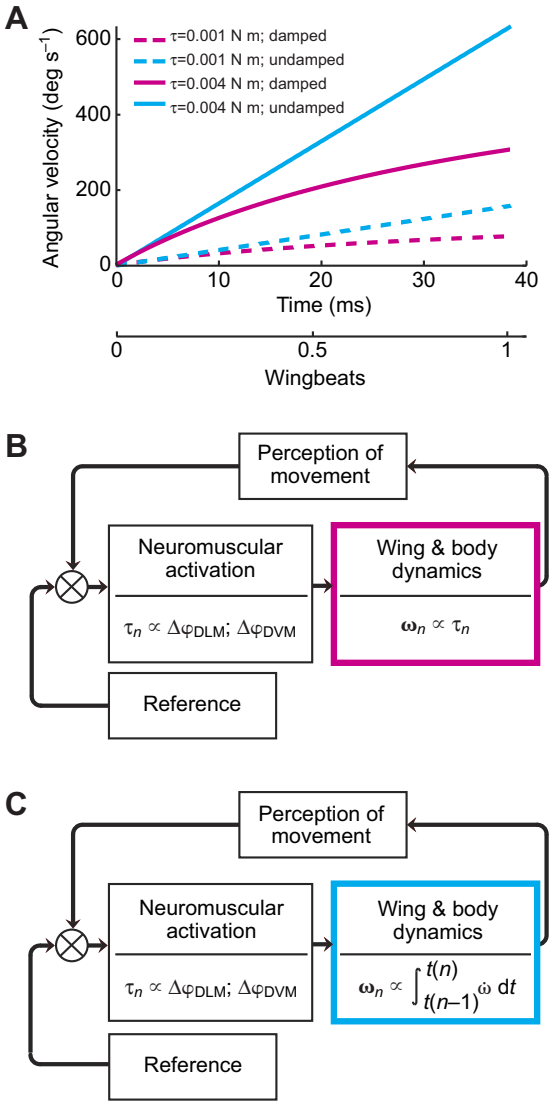

Fig. 1. (A) Analytic solutions to Eqn 4, using values for moment of inertia I, constant b_{ω} and torque τ relevant to *Manduca sexta*, demonstrate the dynamical differences in damped and undamped systems. Cyan lines illustrate rotational dynamics in a completely undamped scenario (b_{ω}=0). A non-zero damping coefficient, illustrated by the magenta lines, causes the rotational velocity to asymptotically approach a steady-state value. An empirically determined value of b_{ω} for *M. sexta* (Hedrick et al., 2009) produces a decay half-life of approximately 0.7 wingbeats (30 ms), which is independent of the applied torque. (B,C) Two possible control architectures: a damping-dominated system, which requires only a torque input to achieve a newly specified angular velocity (B) and an inertia-dominated system which also requires information on the moth's current state or prior wingbeats to control angular velocity (C).

Specifically, we simultaneously made extracellular muscle activation recordings and acquired body kinematics of *Manduca sexta* (L.) during free-flight yaw turns. We used freely flying subjects, rather than those attached to rigid tethers, to preserve the full aerodynamic effects of FCT. Free-flight preparations also maintain natural sensor–motor feedback, reducing the likelihood that our results will be distorted by aberrant or exaggerated behaviours, which are sometimes observed in rigidly tethered animals (Wang

et al., 2008). We correlate dorsal longitudinal muscle (DLM; wing depressor muscle) and dorsal ventral muscle (DVM; wing elevator muscle) bilateral activation phase differences with yaw velocity and yaw acceleration. Though the DLM and DVM have historically been categorized as 'power' muscles (Pringle, 1957), there is growing evidence (Sponberg and Daniel, 2010; Tu and Daniel, 2004; Wang et al., 2008) that flying insects with synchronous flight muscles (e.g. moths) may, like vertebrate flyers (Hedrick and Biewener, 2007b), modulate main flight muscle power output during manoeuvres.

MATERIALS AND METHODS

Subjects

We chose *M. sexta* for this study because it is a large insect with synchronous flight muscles capable of complex manoeuvres, including prolonged stable hovering. All these traits simplify collection of neuromuscular activation data from freely behaving animals. Additionally, their widespread cultivation in a laboratory setting and study by numerous researchers offer ample anatomical and physiological references. Earlier studies of neural control of flight in both tethered (e.g. Kammer, 1971) and freely flying contexts (e.g. Wang et al., 2008) provide many opportunities for comparison of our results with those of other researchers.

We gathered male and female *M. sexta* as pupae from a domestic colony maintained by the Duke University Department of Biology. Pupae and adult moths were housed in 30×30×30 cm mesh cages inside an environment chamber. We maintained the moths on a 22 h:2 h light:dark cycle to reduce wear on their wings. Individuals were differentiated using a small amount of enamel paint applied to the abdomen tip.

Beginning 2–3 days after eclosion, we presented moths with both natural and artificial flowers to elicit feeding behaviour. Suitable feeding behaviour consisted of sustained (longer than 10 s), stable hovering and tracking of the feeding target. Though occurring naturally in *M. sexta*, we reinforced this behaviour with a food reward consisting of 1:4 honey:water mixture. Moths became candidates for electrode implantation once they demonstrated consistent flight and feeding behaviour.

Electrode implantation

Prior to electrode implantation, we placed the subject in a chilled (5°C) enclosure until quiescent (typically between 4 and 10 min). Once quiescent, the moth was restrained, using padded clamps over its wings, on a chilled operating table such that the dorsal surfaces of the thorax and abdomen were accessible. We removed scales obscuring the areas of implantation using forceps and compressed air.

To ease the insertion of electrodes, we first made a circular incision, 0.25 mm in diameter, through the exposed cuticle over each muscle of interest (Fig. 2). We then inserted a 1–2 mm long, 0.1 mm diameter tungsten electrode (A-M systems, Inc., Carlsborg, WA, USA), electrically and physically bonded to a 1 m long signal wire (0.15 mm diameter, copper, enamel coated; EIS/Fay Electric Wire, Elmhurst, IL, USA), through each incision and into the muscle tissue.

We secured all electrodes to the animal at the insertion site with a combination of cyanoacrylate adhesive (Loctite Super Glue; Henkel Corp., Avon, OH, USA) and sodium bicarbonate. To limit motion artefacts created by the animal's movement and to improve electrode longevity through reduced strain at the insertion site, we additionally secured the signal wires to the tip of the abdomen with the same adhesive technique, allowing sufficient slack between the two attachment sites to permit normal abdominal flexion and other postural movements.

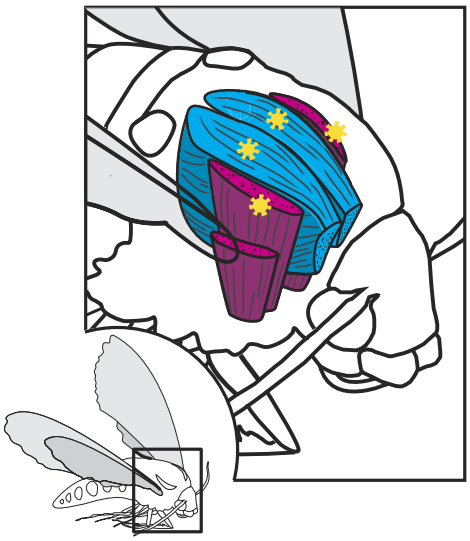

Fig. 2. Anatomy of the main flight muscles in *M. sexta*. The dorsal longitudinal muscle (DLM, cyan), responsible for downstroke, lies parallel to the anteroposterior axis in the medial region of the thorax. The dorsal ventral muscle (DVM, magenta), responsible for upstroke, lies parallel to the dorsoventral axis in the lateral region of the thorax. Approximate implantation sites are indicated in yellow.

Acquisition of muscle activation phases

We placed a single electrode in four separate flight muscles, the left DLM, left DVM, right DLM and right DVM. We connected ipsilateral electrodes (e.g. left DLM and left DVM) to a differential amplifier (gain ×100, analog filters 10 Hz to 10 kHz bandpass, 60 Hz notch; Model 1800; A-M Systems, Inc.) as shown in Fig. 3. A 14-bit data acquisition system (USB-6251; National Instruments, Austin, TX, USA), operating at 15 kHz per channel, digitized and saved all amplified electromyograms (EMGs). As the DVM and DLM are not co-activated in flight, this method essentially produces a single signal, which is a superposition of two, opposite-polarity, single-point recordings from the two muscles. The DLM and DVM signals can then be distinguished during the analysis stage by comparing recorded EMGs with corresponding video data; DLM signals precede downstroke while DVM signals precede upstroke (Kammer, 1967). Although this is an unconventional electrode configuration, it reduces the number of required implantations, the handling time and the additional mass the moth must carry (Wang et al., 2008).

We processed the EMG data to extract activation phase relative to the wingbeat (Fig. 3). Activation phase has been correlated with wing kinematic changes in hawkmoths (Kammer, 1971; Rheuben and Kammer, 1987) and expression of activation timing in terms of wingbeat phase automatically normalizes the data with regard to changes in wingbeat frequency. We extracted phase by first applying a bandpass, 4th-order Butterworth filter (200 Hz to 600 Hz) to each EMG signal, and then using a semi-automated spike detection routine to extract the raw activation times. We converted these times into left–right phase differences, $\Delta\varphi_{n,DLM}$ and $\Delta\varphi_{n,DVM}$, relative to wingbeat period as per the following equation:

$$\Delta\varphi_{n,\text{muscle}} = \frac{t_{n,\text{muscle,L}} - t_{n,\text{muscle,R}}}{T_n} , \quad (6)$$

where t is the measured time of muscle activation for the relevant muscle (subscripts L and R denote left and right sides, respectively,

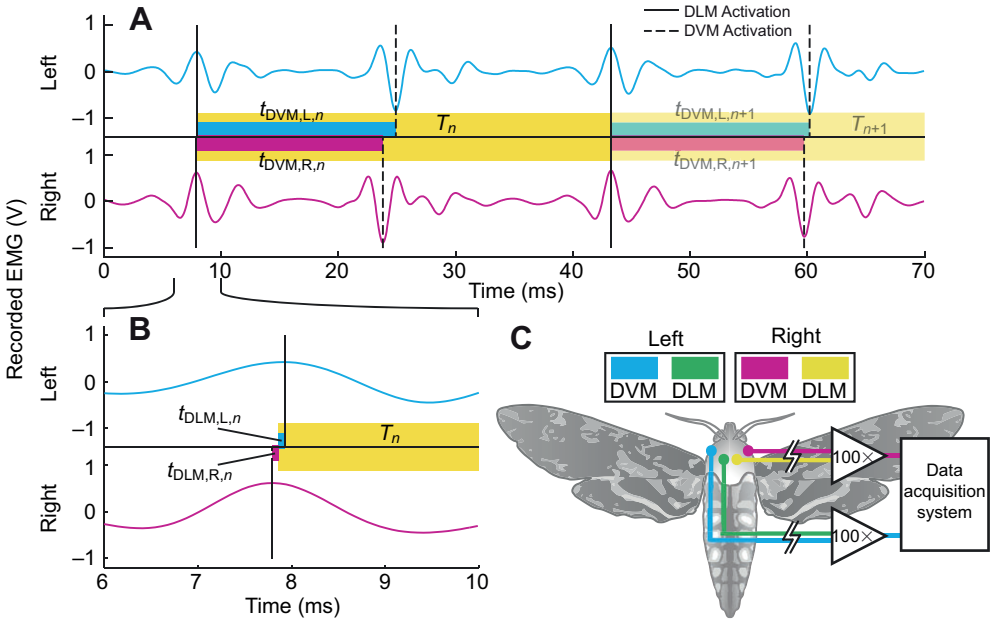

Fig. 3. Example electromyogram (EMG) data showing activation phase extraction (A,B) and a diagram of the EMG acquisition set-up (C). Wingbeat period, T_n (yellow bar), is defined here to begin at the left–right average DLM activation time and extend to the subsequent average DLM activation time. Muscle activation timings for a given wingbeat, $t_{DVM,L,n}$, $t_{DVM,R,n}$, $t_{DLM,L,n}$ and $t_{DLM,R,n}$ [cyan and magenta bars for left (L)- and right (R)-side events, respectively], are defined as the time difference between activation and the start of that wingbeat.

n denotes the nth wingbeat), and T is the wingbeat period, defined here as the time between two subsequent left/right average DLM activation events:

$$T_n = \left(\frac{t_{n+1,\mathrm{DLM,L}} + t_{n+1,\mathrm{DLM,R}}}{2}\right) - \left(\frac{t_{n,\mathrm{DLM,L}} + t_{n,\mathrm{DLM,R}}}{2}\right). \quad (7)$$

This period, T_n, also defines the start and end of wingbeats for the kinematic data described subsequently.

Kinematics and behaviour

Three high-speed video cameras (two Phantom v7.1 and one Phantom v5.1; Vision Research, Wayne, NJ, USA) operating at either 500 or 1000 frames s^{-1} (shutter duration between 700 and 990 µs) recorded the moths. A set of eight custom-made high-intensity LED lamps provided additional near-infra-red (760 nm) illumination. The camera activity signal, recorded with the same analog-to-digital acquisition system as the electrophysiological data, provided temporal synchronization between video and EMG data.

The cameras were calibrated for 3D kinematic reconstruction *via* a direct linear transform and kinematics acquired using the DLTdv5 package for MATLAB (Hedrick, 2008). We reconstructed the moth's yaw orientation for each video frame from the head and abdomen positions (Fig. 4), filtered using a smoothing spline with error tolerances provided by the 3D reconstruction error in the three-camera stereo array (Hedrick, 2008). Differentiation of the resulting spline polynomials provided yaw velocity and yaw acceleration, allowing us to extract kinematic values at specific times (e.g. yaw velocity at the beginning or end of a wingstroke, with beginning and end defined by DLM activation as described above).

Experimental protocol

Following implantation, the moths were allowed to recover for a minimum of 1 h, after which they were placed inside a 0.7×0.7×0.7 m chamber and recording commenced. We elicited flight by presenting natural and artificial flowers and/or applying gentle pressure to the moth's abdomen. Once active, we allowed the moth to fly in a self-selected fashion while continuously acquiring video and EMG data. Moths that were unable to achieve flight performance similar to that exhibited in training, as a result of additional mass from the implant, motion constraints imposed by the signal wires, substantial handling during the implantation process or some other factor, were given a further recovery period or discarded. We saved only recordings in which the moth demonstrated a substantial yaw turn with minimal additional manoeuvring and without external interference such as physical contact between the moth's proboscis and the flower.

Analysis and statistics

The basic observational unit in this study is a time series of successive wingbeats. For each wingbeat, we considered initial and final yaw velocities along with muscle activation timing differences.

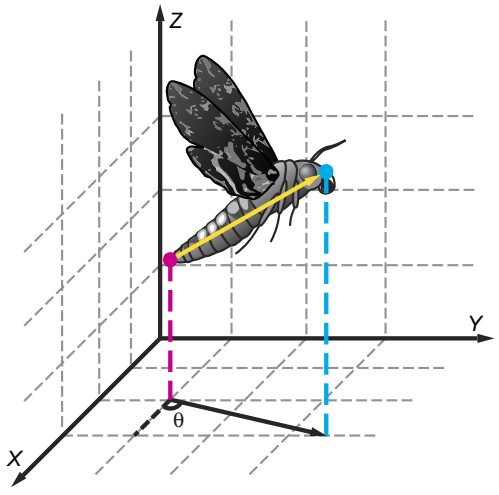

Fig. 4. Body tracking scheme and yaw orientation extraction. We tracked points on the moth's head and abdomen (cyan and magenta circles, respectively) and reconstructed their locations in the global 3D coordinate system *XYZ*. These two points produce a vector, shown in yellow, which represents the moth's position and orientation in that frame of the video (yellow arrow). Yaw, θ, is found by converting this vector from Cartesian to polar coordinates.

Different time series of varying lengths were obtained from the same individual on different occasions (trials) as well as from different individuals. To assess the effects of initial velocity, phase differences in the DLM and phase differences in the DVM on the final velocity reached by the moth during each wingbeat, we fitted a linear mixed-effects model using the nlme package of R 2.12 (Pinheiro et al., 2009; R Development Core Team, 2011). Using these data for all individuals and trials, we fitted four mixed models: damping-dominated (predicts final velocity, $\omega_{n,\mathrm{final}}$, from only muscle activation, $\Delta\varphi_{n,\mathrm{DLM}}$ and $\Delta\varphi_{n,\mathrm{DVM}}$), inertia-dominated (predicts $\omega_{n,\mathrm{final}}$ from initial velocity, $\omega_{n,\mathrm{initial}}$, and muscle activation, $\Delta\varphi_{n,\mathrm{DLM}}$ and $\Delta\varphi_{n,\mathrm{DVM}}$), a control–neutral, or null, model (predicts $\omega_{n,\mathrm{final}}$ from $\omega_{n,\mathrm{initial}}$ only), and a combined model (predicts $\omega_{n,\mathrm{final}}$ from both muscle activation, $\Delta\varphi_{n,\mathrm{DLM}}$ and $\Delta\varphi_{n,\mathrm{DVM}}$, and $\omega_{n,\mathrm{initial}}$). We then compared the predictive power and Akaike's information criterion (AIC, see below) of each model to judge which most accurately reflected the actual control relationship. A detailed explanation of the formulation of each of these models from Eqns 1–5 is given in the Appendix.

To address the repeated measures within trials and to account for the unbalanced nature of the data, we used a random intercepts model in which observations coming from the same moth were assigned the same random effect (Pinheiro and Bates, 2000). Although trials were also nested in moths, we did not assign a random effect to trials because all trials tend to have a non-zero average yaw velocity, which is removed by a per-trial random factor. As non-zero average yaw velocities are consistent with both damping and inertia-dominated motion models, we left them intact by restricting random factors to moths only. The data also did not support treating additional parameters beyond the intercepts as random.

Models were fitted using maximum likelihood and the best predictor set was determined using AIC, an information-theoretic measure in which a model's log-likelihood is penalized by the number of estimated parameters used (Burnham and Anderson, 2002). The best model among a set of candidate models is the one with the smallest AIC value. Analysis of the autocorrelation function (ACF) and partial autocorrelation function (PACF) of the level-1 residuals of the AIC best model revealed a significant temporal autocorrelation that approximated a first-order auto-regressive AR(1) process. Consequently an AR(1) correlation structure for the residuals was added to each of the random intercepts models. In the final model, all the reported terms were judged statistically significant at α=0.05.

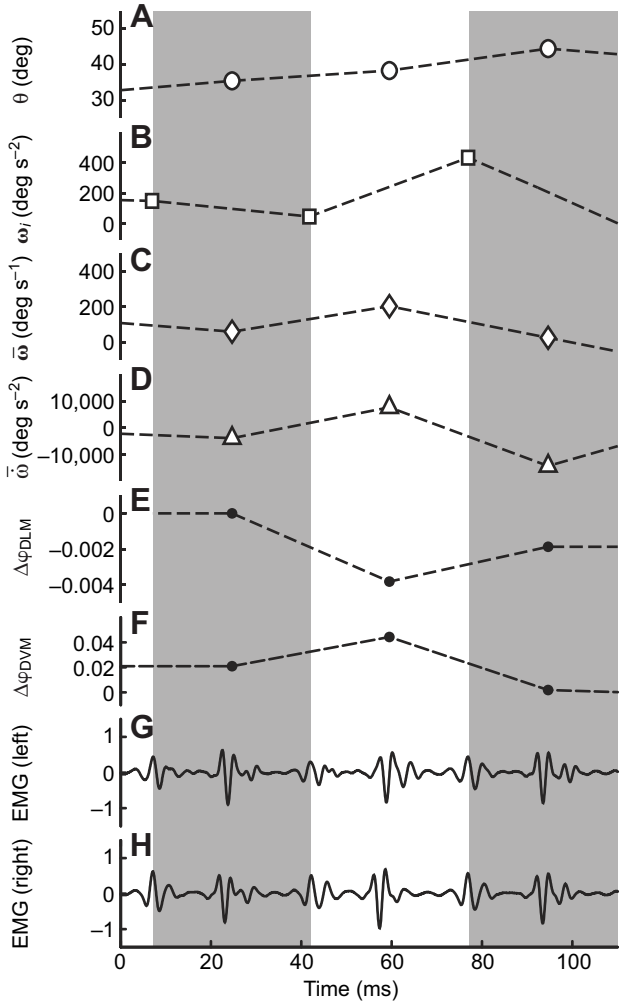

Fig. 5. Mean yaw orientation (A), initial yaw velocity (B), mean yaw velocity (C), mean yaw acceleration (D), DLM phase difference (E), DVM phase difference (F) and EMGs (G,H) for three consecutive wingbeats within a single trial. During this portion of the trial, the moth performed a turn to its right.

RESULTS

Overview of measurements

Using bilateral combined DLM/DVM recording techniques, we examined 5 individuals making 22 yaw turns over a total of 455 individual wingbeats. Recorded manoeuvres included stationary hovering, and both left and right yaw turns with maximum speeds distributed between 0 and 1000 deg s^{-1}. Fig. 5 shows representative data from a single trial.

Model comparison

We found statistically significant correlations in each of our candidate models (Table 1). However, the fit of each of these models to the observed kinematics varied greatly.

The damping-dominated model, which represents a case where neuromuscular input is directly proportional to yaw velocity, found that final yaw velocity was significantly associated with both DLM activation phase difference (LME, t=3.457, P=0.0006) and DVM phase (LME, t=7.363, P<0.0001, Table 1). Despite statistical significance, this model performed poorly when compared with the moth's actual motion (Fig. 6A).

The inertia-dominated model, which represents a system where damping does not significantly influence rotational acceleration, found that DVM activation phase difference had a significant effect on final yaw velocity (LME, t=3.423, P=0.0007). In this case, however, DLM phase difference was not significantly associated with the model (LME, t=0.004, P=0.997, Table 1). Again, despite the statistical significance of the correlation, this model also weakly predicted the observed motion (Fig. 6B). Note that the inertia-dominated model includes the initial yaw velocity of each wingbeat. However, there is no coefficient associated with this term so it does not contribute to the AIC.

The control–neutral model, which uses only initial velocity to predict final velocity, disregarding muscle activation data, found that initial velocity was significantly correlated with final velocity in these data (LME, t=26.528, P<0.0001, Table 1). Although this model does not consider any input from the moth's neuromuscular system, it fits the observed kinematics better than the previous two models (Fig. 6C).

Table 1. Results from each mixed-effects model

Model type		Value	s.e.m.	d.f.	*t*	*P*
Damping dominated	Intercept	41.226	17.895	454	2.304	0.022
	DLM	2270.004	656.579	454	3.457	0.0006
	DVM	2637.813	358.242	454	7.363	<0.0001
Inertia dominated	Intercept	3.339	5.8819	454	0.568	0.570
	DLM	2.249	609.385	454	0.004	0.997
	DVM	1266.050	369.980	454	3.423	0.0007
Control–neutral	Intercept	18.705	6.954	455	2.690	0.007
	Velocity	0.723	0.027	455	26.528	<0.0001
Combined	Intercept	12.943	5.618	453	2.304	0.022
	Velocity	0.653	0.028	453	23.472	<0.0001
	DLM	1374.714	567.932	453	2.420	0.016
	DVM	2332.111	342.617	453	6.807	<0.0001

DLM, dorsal longitudinal muscle: DVM, dorsal ventral muscle.

Value and s.e.m., respectively, represent the fixed effects coefficients and their standard errors. These give the slope of the relationship between independent and dependent variables in the complete, hierarchical model. The *t*-value is the ratio between the estimates and their standard errors and the *P*-value is the associated *P*-value from a *t*-distribution; results may be considered significant at $P<0.05$. Moths were included as random components in all models. $N=5$ individuals and $n=461$ observations (wingbeats).

Finally, the combined model, which includes both muscle activation timing differences and initial velocity as predictors of final velocity, found that all three predictors were significantly correlated with the final velocity for that wingbeat (LME, initial velocity: $t=23.472$, $P<0.0001$; DLM: $t=2.420$, $P=0.016$; DVM: $t=6.807$, $P<0.0001$; Table 1). The sign of the coefficients for DLM and DVM activation timing differences both indicate that asymmetric activation is associated with a turn towards the muscle

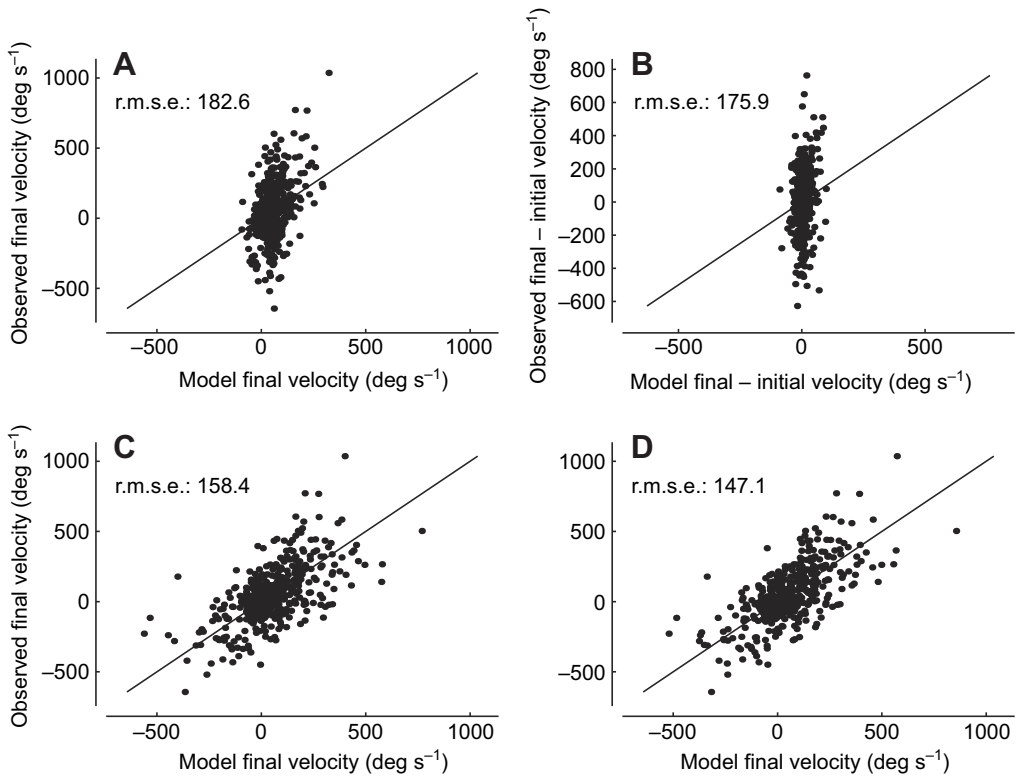

Fig. 6. Comparison of the observed and fitted results for each of the four models over all recorded wingbeats, along with the root mean square error (r.m.s.e.) between model and observation, and a dashed line with a slope of one and intercept of zero. Fitted values were extracted from the linear mixed effects model with autocorrelation adjustment. This includes a random factor for each individual moth but otherwise fits a single value to each free coefficient in the characteristic equation (see Appendix for the exact equations in each model). Damping-dominated, inertia-dominated, control–neutral and combined models are shown in A–D, respectively. The inertia-dominated model fits final velocity from initial velocity and EMG phase. Because initial velocity does not have an associated coefficient in this model, all information is added by the EMG term only. Thus, we display the results of this model as the relationship between the observed and model difference in final and initial velocities. The EMG-based models, A and B, both exhibit a poor fit between model and data. The combined model, D, which explicitly includes damping and EMG factors, performed best here and in the AIC comparison (Table 2). However, it is only a modest improvement over the control–neutral model, C, indicating that damping is a crucial contributor in explaining the relationship between neuromuscular activity and movement in *M. sexta*.

Table 2. AIC for each model

Model	AIC
Damping dominated	5954
Inertia dominated	6019
Control–neutral	5940
Combined	5892

AIC, Akaike's information criterion.
Lower values indicate better agreement between the model and data.

that was activated first (e.g. activation of the right DVM before the left DVM is correlated with a turn to the right). This model yields the best overall fit to the moths' observed motion (Fig. 6D) and also had the smallest (i.e. best) AIC (Table 2). Thus, among the models presented here, it best represents the relationship between the moths' neural inputs and turning behaviour. Data from all measurements used in these models are available in supplementary material Table S1.

DISCUSSION

In this study, we correlated flight muscle activation timing differences with behavioural kinematics in freely flying moths to determine how passive damping influences the control of planar yaw turns. We tested our initial hypothesis that passive damping from FCT reduces yaw control to a damping-dominated regime where muscle torques directly prescribe final angular velocity on a wingbeat by wingbeat basis by fitting a linear model (A) associating observed yaw manoeuvring velocities with muscle activation timing differences alone. We also tested additional models that fitted manoeuvring velocities (B) from muscle activation in conjunction with initial wingbeat velocity, (C) from initial yaw velocity and a damping coefficient (a control–neutral model), and (D) from both damped initial velocity and muscle activation. The poor fit of models A and B where kinematics are associated with muscle activation alone (Table 1, Fig. 6) suggests that flapping-flight yaw turns lie in neither an extreme damping nor inertia-dominated control domain. Instead, our data best support mixed control model D where the animal produces momentary torques that lead to within-stroke accelerations but simultaneously experiences substantial damping. Inclusion of this damping in a neuromechanical model of flight control is crucial for interpreting the effect of neural outputs on manoeuvring flight. Analyses that consider only the neural data explain little of the overall behaviour (Fig. 6A,B), as much of the observed dynamics are due to damping (Fig. 6C).

Our findings are consistent with mathematical models for FCT that predict a damping half-life of 0.7 wingbeats for *M. sexta* (Hedrick and Robinson, 2010), matched by the values of 0.72 and 0.65 for the velocity coefficient in statistical models C and D, which include a damping term (Table 1). However, this result is somewhat surprising because the moths are neither exploiting damping forces to simplify turning control on a wingbeat to wingbeat time scale nor avoiding the potential increase in locomotor energy requirements caused by constant damping.

The importance of both damping and inertial effects in the neuromechanics of hawkmoth yaw turns has several possible explanations, including the following. (1) FCT damping is an inherent feature of flapping flight that is undesirable from a manoeuvring and efficiency standpoint, but reducing FCT is costly for other reasons. For instance, reducing damping might require changes to morphology that increase the inertial power requirements of flight (Weis-Fogh, 1973) or produce other undesirable consequences. In this case, we expect similar control relationships among flying animals regardless of flight performance requirements. (2) Alternatively, damping and inertia-dominated systems represent the two extremes of a scale where an animal trades manoeuvrability for stability. Thus, the moth's position at the midpoint of the two extremes may represent a compromise between providing stability against external perturbations and simultaneously providing adequate manoeuvrability to fly in a cluttered environment and avoid predators. In this case, neuromechanical control relationships and their interaction with damping are likely to vary widely among species.

The degree to which animals exhibit damping or inertia-dominated neuromuscular to manoeuvring relationships also depends on the time scale of damping as compared with manoeuvring inputs. In the case of a moth, damping occurs on approximately the same time scale as a single wingbeat, the time scale at which the moth varies its neuromuscular inputs (Fig. 5). However, this ratio may vary substantially among all flying animals. Fruit flies and other insects with asynchronous flight muscle may have only limited neuromuscular control of individual wingbeats (Heide, 1983), while bats and birds may vary neuromuscular activity within a single wingbeat (Warrick et al., 1998). However, birds and bats also experience greater damping in a non-dimensional time scale than fruit flies (Hedrick et al., 2009). In general, we expect that reducing passive dynamics time scales *via* the introduction of damping or self-correcting mechanisms such as those due to FCT or demonstrated in simulations of rapid hexapedal locomotion (Kubow and Full, 1999) will favour damping-dominated control of locomotion, but faster neuromuscular time scales would favour inertia-dominated control. Thus, the trends in neuromuscular and body dynamics time scales in flying animals act in opposite directions, leaving open the question of whether the damped neuromuscular control relationship found here is typical of most flying animals or is particular to *M. sexta*.

Role of DLM and DVM in flight control

As described above, our results demonstrate an association between DLM and DVM phase differences and turning flight. They do not, however, show that the DLM and DVM directly produce turns, although there is increasing evidence that this is the case. Wang et al. (Wang et al., 2008) found a correlation between DVM activation and changes in the stroke plane angle; Sponberg et al. (Sponberg and Daniel, 2010; Sponberg et al., 2012) directly correlated yaw torque production and DLM phase differences in tethered hawkmoths; and Bozkurt et al. (Bozkurt et al., 2009) observed yaw turn wing kinematics following direct stimulation of the DLM and DVM in tethered hawkmoths. Nevertheless, other flight muscles, most notably the third axillary, have also been correlated with changes in wing flapping kinematics in both tethered and freely flying hawkmoths (Rheuben and Kammer, 1987; Wang et al., 2008) and it is likely that information from these muscles, along with simultaneous information from the DLM and DVM, is required for a full understanding of how hawkmoths create asymmetric aerodynamic forces. For instance, DLM and DVM modulation may occur if additional muscle force is required to produce a yaw torque while simultaneously maintaining the same average lift on the left and right wings. However, even in these scenarios where a suite of muscles is co-activated to produce yaw turns, our overall finding that the relationship between neural inputs to the flight musculature remains intact as although the DLM and DVM may not be directly causal to turning, they are a necessary part of it.

This finding represents a departure from the traditional categorization of muscles as either 'power' or 'steering' in

synchronous fliers such as Lepidoptera. The traditional categorization may, however, still be appropriate for asynchronous fliers (e.g. dipterans, hymenoptera) as their wingbeat frequency exceeds the maximum rate of neurogenic activation, making direct associations between DLM or DVM timing and manoeuvres unlikely.

Future work

It remains to be shown how advancing the activation of indirect flight muscles can produce asymmetric aerodynamic forces in free flight. An investigation, conducted while the moth is engaged in stationary hovering, where the natural activation of the DVM is overwritten with an artificial signal (e.g. Sponberg et al., 2011) would permit correlation of within-wingbeat body and wing kinematics with muscle activation phase. By stimulating only the indirect flight muscles, we may be able to isolate their effects from those of the typically co-activated direct flight muscles. Similar investigations, conducted on a wide range of flight muscles, may reveal the extent to which each muscle contributes to a variety of behaviours.

APPENDIX

Here, we present a description of the mathematical models underlying the different yaw turning relationships examined *via* statistical analysis of observed hawkmoth flight kinematics and neuromuscular activity in this study.

A complete general description of the yaw turn dynamics of the moth is given by:

$$\dot{\omega} = \frac{\tau - b_\omega \boldsymbol{\omega}}{I} , \quad \text{(A1)}$$

where $\dot{\omega}$ is angular acceleration, τ is torque, b_ω is a constant, $\boldsymbol{\omega}$ is angular velocity and I is the yaw moment of inertia. In the models for how the moth might control its manoeuvres, we compare predictions of the moth's angular velocity at the end of its flapping cycle, i.e. we integrate Eqn A1 over time:

$$\boldsymbol{\omega}_{\text{final}} = \int_0^t \dot{\omega} , \quad \text{(A2)}$$

and consider the exact form of Eqn A2 for different assumptions as to the importance of the different terms in Eqn A1. At this step the general and continuous time model given in Eqn A1 is converted to a discrete model, eventually leading to predictions for the outcome of a single, finite locomotor cycle given a set of neuromuscular inputs and initial conditions. This is done to match the model to the experimental recordings, which are composed of a time series of discrete flapping cycles with differing and uncorrelated neural inputs.

As is shown in Eqn A2, the duration of application of the torque clearly influences our predictions. However, from a practical standpoint, the measured neural inputs of the moth change from flap to flap, but the flap duration was similar throughout the experiment and for all moths (36.7±1.9 ms, n=483, mean ± s.d.). Thus, from this point forward we assume that duration does not vary, i.e. t is constant.

Furthermore, throughout this exercise, we assume that the torque produced by the moth's flight muscles during a complete flapping cycle is a linear function of the left–right phase differences of the two pairs of flight muscles, the DLM and DVM. Thus, torque is given by:

$$\tau = k_1 \Delta\phi_{\text{DLM}} + k_2 \Delta\phi_{\text{DVM}} , \quad \text{(A3)}$$

where k_1 and k_2 are constants and $\Delta\varphi_{n,\text{DLM}}$ and $\Delta\varphi_{n,\text{DVM}}$ indicate the phase differences between left and right DLM and DVM, respectively.

Damping-dominated model

In the damping-dominated model we consider the case where b_ω is much larger than I. In this case the moth accelerates to the angular velocity at which $\tau = b_\omega \boldsymbol{\omega}$ and no further acceleration is possible. Thus:

$$\boldsymbol{\omega}_{\text{final}} = \frac{k_1 \Delta\phi_{\text{DLM}} + k_2 \Delta\phi_{\text{DVM}}}{b_\omega} . \quad \text{(A4)}$$

For purposes of statistically relating the angular velocity at the end of the flap to the actions of the moth, there are two free parameters, k_1/b_ω and k_2/b_ω, which may vary among moths given slight differences in neuromuscular implant positioning and individual variation in the damping coefficient b_ω.

Inertia-dominated model

The inertia-dominated model considers the opposite case of the prior model, one where b_ω is negligible compared with I in Eqn A1. In this case, solving the integral in Eqn A2 results in:

$$\boldsymbol{\omega}_{\text{final}} = t\left(\frac{k_1 \Delta\phi_{\text{DLM}} + k_2 \Delta\phi_{\text{DVM}}}{I}\right) + \boldsymbol{\omega}_{\text{initial}} , \quad \text{(A5)}$$

where $\boldsymbol{\omega}_{\text{initial}}$ is the moth's yaw velocity at the beginning of the flapping cycle. With respect to the statistical analysis, Eqn A5 also has two independent parameters that may be expected to vary from moth to moth but instead of predicting $\boldsymbol{\omega}_{\text{final}}$ from the muscle activation timing data alone, it essentially predicts the difference between $\boldsymbol{\omega}_{\text{final}}$ and $\boldsymbol{\omega}_{\text{initial}}$, i.e. the moth's angular acceleration assuming constant stroke duration.

Control–neutral model

We introduce the control–neutral model to represent cases where the modulation of DLM and DVM activation timing does not relate to the torque produced by the moth as described in Eqn A3. In this case, from a statistical standpoint:

$$\boldsymbol{\omega}_{\text{final}} = k_3 \boldsymbol{\omega}_{\text{initial}} , \quad \text{(A6)}$$

where k_3 is a constant incorporating the expected decay half-life for Eqn A1 at a fixed time interval. Thus, k_3 is expected to be less than one but may vary among moths.

Combined model

Our combined model simply incorporates all terms from Eqn A1, assuming that torque production and damping are both important components of the observed dynamics and that the DLM and DVM timing differences do relate to the torque produced by the moth. In this case:

$$\boldsymbol{\omega}_{\text{final}} = k_1 \Delta\varphi_{\text{DLM}} + k_2 \Delta\varphi_{\text{DVM}} + k_3 \boldsymbol{\omega}_{\text{initial}} , \quad \text{(A7)}$$

Thus, for the combined model there are three free parameters to be estimated from the data. Note that k_1 and k_2 in Eqn A7 include the effects of flapping cycle duration, moment of inertia and damping as well as a muscle phase difference to torque relationship. As before, all coefficients may vary among moths and k_3 is expected to be less than one.

As noted in the Materials and methods, we use the AIC to identify the model that best describes the relationship between the moth's angular velocity at the end of the flapping cycle, its initial angular velocity, and the activation phase differences between the left and right DLM and DVM pairs. Because the models do not all incorporate the same number of free parameters, it is possible for a model to better fit the final velocity from its inputs but have a worse AIC.

Finally, while the different statistical models do provide grounds for moth-level random effects, i.e. differences among moths, they do not support the use of trial-level random effects as outputs from the underlying physical parameters that may give rise to differences among individuals are not expected to vary among trials from the same individual.

LIST OF SYMBOLS AND ABBREVIATIONS

ACF	autocorrelation function
b_ω	constant coefficient
DLM	dorsal longitudinal muscle
DVM	dorsal ventral muscle
EMG	electromyogram
FCT	flapping counter-torque
I	moment of inertia
n	nth wingbeat
PACF	partial autocorrelation function
t	time
T	wingbeat period
$\Delta\varphi_{DLM}$	DLM phase difference
$\Delta\varphi_{DVM}$	DVM phase difference
θ	yaw
τ	torque
$\boldsymbol{\omega}$	rotational velocity
$\boldsymbol{\omega}_i$	initial velocity
$\boldsymbol{\omega}_{n,final}$	final velocity
$\boldsymbol{\omega}_{n,initial}$	initial velocity
$\boldsymbol{\omega}_s$	saturation velocity
$\dot{\omega}$	rotational acceleration

ACKNOWLEDGEMENTS

We wish to thank M. Ellis Driver for assistance with figures, Laura Pianowski for assistance in the experiments and video analysis, Jack Weiss for assistance with statistical analyses, and Monica Daley for valuable discussion. Two anonymous referees contributed insightful comments that greatly improved the manuscript. Hawkmoths were provided courtesy of F. Nijhout at Duke University.

FUNDING

Funding was provided by the National Science Foundation [grant no. IOS-0920358 to T.L.H.].

REFERENCES

Åström, K. J. and Murray, R. M. (2008). *Feedback Systems: An Introduction for Scientists and Engineers*. Princeton, NJ: Princeton University Press.
Balint, C. N. and Dickinson, M. H. (2004). Neuromuscular control of aerodynamic forces and moments in the blowfly, *Calliphora vicina*. *J. Exp. Biol.* **207**, 3813-3838.
Bozkurt, A., Gilmour, R. F., Sinha, A., Stern, D. and Lal, A. (2009). Insect-machine interface based neurocybernetics. *IEEE Trans. Biomed. Eng.* **56**, 1727-1733.
Burnham, K. P. and Anderson, D. R. (2002). *Model Selection and Multimodel Inference*. New York, NY: Springer-Verlag.
Cowan, N. J. and Fortune, E. S. (2007). The critical role of locomotion mechanics in decoding sensory systems. *J. Neurosci.* **27**, 1123-1128.
Cowan, N. J., Lee, J. and Full, R. J. (2006). Task-level control of rapid wall following in the American cockroach. *J. Exp. Biol.* **209**, 1617-1629.
Dickinson, M. H., Farley, C. T., Full, R. J., Koehl, M. A. R., Kram, R. and Lehman, S. (2000). How animals move: an integrative view. *Science* **288**, 100-106.
Fry, S. N., Rohrseitz, N., Straw, A. D. and Dickinson, M. H. (2009). Visual control of flight speed in *Drosophila melanogaster*. *J. Exp. Biol.* **212**, 1120-1130.
Full, R. J., Stokes, D. R., Ahn, A. N. and Josephson, R. K. (1998). Energy absorption during running by leg muscles in a cockroach. *J. Exp. Biol.* **201**, 907-1012.
Hedrick, T. L. (2008). Software techniques for two- and three-dimensional kinematic measurements of biological and biomimetic systems. *Bioinspir. Biomim.* **3**, 034001.
Hedrick, T. L. and Biewener, A. A. (2007a). Experimental study of low speed turning flight in cockatoos and cockatiels. AIAA Paper 2007-0044. AIAA Aerospace Sciences Meeting and Exhibit, 8-11 January 2007, Reno, NV, USA.
Hedrick, T. L. and Biewener, A. A. (2007b). Low speed maneuvering flight of the rose-breasted cockatoo (*Eolophus roseicapillus*). I. Kinematic and neuromuscular control of turning. *J. Exp. Biol.* **210**, 1897-1911.
Hedrick, T. L. and Robinson, A. K. (2010). Within-wingbeat damping: dynamics of continuous free-flight yaw turns in *Manduca sexta*. *Biol. Letters* **6**, 422-425.
Hedrick, T. L., Cheng, B. and Deng, X. (2009). Wingbeat time and the scaling of passive rotational damping in flapping flight. *Science* **324**, 252-255.
Heide, G. (1983). Neural mechanisms of flight control in Diptera. In *BIONA Report* (ed. W. Nachtigall). Stuttgart: Fischer Verlag.
Josephson, R. K. (1985). Mechanical power output from striated muscle during cyclical contraction. *J. Exp. Biol.* **114**, 493-512.
Kammer, A. E. (1967). Muscle activity during flight in some large *Lepidoptera*. *J. Exp. Biol.* **47**, 277-295.
Kammer, A. E. (1971). The motor output during turning flight in a hawkmoth, *Manduca sexta*. *J. Insect Physiol.* **17**, 1073-1086.
Kubow, T. M. and Full, R. J. (1999). The role of the mechanical system in control: a hypothesis of self-stabilization in hexapedal runners. *Philos. Trans. R. Soc. Lond. B* **354**, 849-861.
Nishikawa, K., Biewener, A. A., Aerts, P., Ahn, A. N., Chiel, H. J., Daley, M. A., Daniel, T. L., Full, R. J., Hale, M. E., Hedrick, T. L. et al. (2007). Neuromechanics: an integrative approach for understanding motor control. *Integr. Comp. Biol.* **47**, 16-54.
Orban, G. A., Hoffmann, K. P. and Duysens, J. (1985). Velocity selectivity in the cat visual system. I. Responses of LGN cells to moving bar stimuli: a comparison with cortical areas 17 and 18. *J. Neurophysiol.* **54**, 1026-1049.
Pinheiro, J. C. and Bates, D. M. (2000). *Mixed-Effects Models in S and S-PLUS*. New York: Springer-Verlag.
Pinheiro, J. C., Bates, D., DebRoy, S., Sarkar, D. and the R Development Core Team (2009). *nlme: Linear and Nonlinear Mixed Effects Models*. R package version 3.1-97. Available from http://cran.r-project.org/web/packages/nlme/index.html.
Pringle, J. W. S. (1957). *Insect Flight*. London: Cambridge University Press.
R Development Core Team (2011). *R: A Language and Environment for Statistical Computing*. R Foundation for Statistical Computing, Vienna, Austria. Available at: http://www.R-project.org.
Rheuben, M. B. and Kammer, A. E. (1987). Structure and innervation of the third axillary muscle of *Manduca* relative to its role in turning flight. *J. Exp. Biol.* **131**, 373-402.
Ristroph, L., Bergou, A. J., Ristroph, G., Coumes, K., Berman, G. J., Guckenheimer, J., Wang, Z. J. and Cohen, I. (2010). Discovering the flight autostabilizer of fruit flies by inducing aerial stumbles. *Proc. Natl. Acad. Sci. USA* **107**, 4820-4824.
Sponberg, S. and Daniel, T. (2010). Phase modulation and control of flight power muscles during visually-induced turning responses in the hawkmoth, *Manduca sexta*. *Integr. Comp. Biol.* **50 Suppl. 1**, e167.
Sponberg, S. and Full, R. J. (2008). Neuromechanical response of musculo-skeletal structures in cockroaches during rapid running on rough terrain. *J. Exp. Biol.* **211**, 433-446.
Sponberg, S., Spence, A. J., Mullens, C. H. and Full, R. J. (2011). A single muscle's multifunctional control potential of body dynamics for postural control and running. *Philos. Trans. R. Soc. Lond. B* **366**, 1592-1605.
Sponberg, S., Daniel, T. L. and Fairhall, A. L. (2012). Using dimensionality reduction to explore muscle synergies and torque encoding during insect flight. Cosyne 2012, Salt Lake City, UT, USA. Available at: www.cosyne.org
Tu, M. S. and Daniel, T. L. (2004). Submaximal power output from the dorsolongitudinal flight muscles of the hawkmoth *Manduca sexta*. *J. Exp. Biol.* **407**, 4651-4662.
Wang, H., Ando, N. and Kanzaki, R. (2008). Active control of free flight manoeuvres in a hawkmoth, *Agrius convolvuli*. *J. Exp. Biol.* **211**, 423-432.
Warrick, D. R., Dial, K. P. and Biewener, A. A. (1998). Asymmetrical force production in the maneuvering flight of pigeons. *Auk* **115**, 916-928.
Weis-Fogh, T. (1973). Quick estimates of flight fitness in hovering animals, including novel mechanisms for lift production. *J. Exp. Biol.* **59**, 169-230.